CAN PLASMA SCATTERING MIMIC A COSMOLOGICAL RED–SHIFT?

S. SCHRAMM* AND S. E. KOONIN

W. K. Kellogg Radiation Laboratory
California Institute of Technology, Pasadena, CA 91125

ABSTRACT

We investigate the extent to which the scattering of light from plasma fluctuations can mimic a cosmological red–shift, as has been suggested by Wolf *et al.* A plasma model for the plasma structure function results in a spectrum of scattered light very different from that associated with a constant red–shift, implying that the "Wolf effect" cannot be involved to perturb the cosmological distance scale.

In a number of articles, Wolf and collaborators have proposed that the scattering of light by a fluctuating medium can shift its frequency in such a way as to mimic a cosmological red–shift (Wolf 1989). This "Wolf effect" has been invoked to explain certain unusual quasar emission features (Arp 1987). In all previous analyses of the phenomenon, the plasma fluctuations have been assumed to be uncorrelated in space and time. Since any interaction of photons with the plasma must have a microscopic origin, it is possible (and indeed essential) to consider whether or not the effect survives when more realistic plasma structure functions are used. Such an investigation is the subject of this paper. Unfortunately, we find that, under plausible circumstances, the spectrum of scattered light differs significantly from that associated with a cosmological red–shift. Hence, the Wolf

* Present address: IUCF, 2401 Milo B. Sampson Lane, Bloomington, IN 47405 USA

effect cannot be invoked to perturb the cosmological distance scale, although it may indeed distort line shapes.

Following the notation in Wolf (1989), we let $S^i(\boldsymbol{u},\omega)$ denote the spectrum of incoming photons with frequency ω and direction $\boldsymbol{u}$ ($\boldsymbol{u}\cdot\boldsymbol{u}=1$). Using standard linear response theory, the scattering properties of the medium can be described by a scattering kernel $\mathcal{K}$ depending upon the momentum $\boldsymbol{q}$ and energy q_0 that the incoming photons deliver to the medium (see Figure 1; we henceforth put $\hbar=c=1$). For a final frequency ω' obtained by scattering through an angle θ, $q_0=\omega-\omega'$ and $|\boldsymbol{q}|^2=\omega'^2+\omega^2-2\omega\omega'\cos\theta$.

The intensity of the light scattered into direction $\boldsymbol{u}'$ with frequency ω' is given by

$$S^f(\boldsymbol{u}',\omega')=A\int_{-\infty}^{\infty}d\omega\;S^i(\boldsymbol{u},\omega)\,\mathcal{K}\left(\omega'\boldsymbol{u}'-\omega\boldsymbol{u},\omega'-\omega,\omega\right) \tag{1}$$

with A an unimportant overall constant. The scattering kernel $\mathcal{K}$ depends upon both the nature and distribution of plasma excitations, as well as the way in which photons couple to them. Wolf *et al.* (1989) assume a Gaussian form for the kernel,

$$\mathcal{K}(\boldsymbol{q},q_0)\sim e^{-\sigma_0^2q_0^2-\sum_i\sigma_i^2q_i^2} \tag{2}$$

with widths $\sigma_0,\sigma_i\,(i=1,2,3)$ for the energy and momentum transfers, respectively. However, since energy and momentum (or space and time) correlations are independent in equation (2), the expression manifestly violates causality and is therefore not a reasonable approximation to a scattering kernel.

To use a more realistic model of the scattering kernel, we consider scattering of light off a gas of non–interacting (quasi–)particles with mass m at a temperature T. At the low momentum transfers associated with optical photons, these excitations are the plasmons,

in which case m is the plasma frequency. The particle distribution is then described by Bose statistics:

$$n(k) = \frac{1}{e^{E_k/T} - 1} \tag{3}$$

and the dispersion relation for the quasiparticles is

$$E_k^2 = k^2 + m^2 \ . \tag{4}$$

The basic scattering process is shown in Figure 1. An incoming photon scatters from a quasiparticle in the medium through an unspecified mechanism Γ. We need not specify the properties of the actual coupling Γ between photons and quasiparticles beyond assuming that any momentum dependence is smooth over the linewidths of interest, as is the case for Thomson scattering.

Under these assumptions, the scattering matrix element is simply $S = \Gamma\, \delta^{(4)}(p' - p + q)$ and the statistical ensemble of quasiparticles generates a scattering kernel of the form

$$\begin{aligned} \mathcal{K}(\boldsymbol{q}, q_0) &= \Gamma^2 \int \tfrac{d^3k}{2E_k}\, n(k) \int \tfrac{d^3k'}{2E_{k'}} \left(\delta^{(4)}(k' - k - q)\right)^2 \\ &= \Gamma^2 \tfrac{VT}{(2\pi)^4} \int \tfrac{d^3k}{2E_k} n(k) \tfrac{1}{2E_{k+q}} \delta(E_k + q_0 - E_{k+q}) \\ &\equiv \tfrac{A}{\omega\omega'} \tilde{\mathcal{K}}(q, q_0) \end{aligned} \tag{5}$$

where V is the normalization volume, $\tilde{\mathcal{K}}$ is independent of ω, and A is a constant.

The temperature dependence of $\tilde{\mathcal{K}}$ is best characterized by $\mu \equiv m/T$. We consider two limiting cases: $\mu = 1$ (relativistic) and $\mu = 10$ (non–relativistic). Figure 2 shows, for these two cases, the scattering kernel $\tilde{\mathcal{K}}$ assuming a mass m of 1 eV. As one can see, $\tilde{\mathcal{K}}$ is not a gaussian, which would have elliptical contours. Further, the kernel is non–zero only in the space–like cone ($q^2 > q_0^2$). In the relativistic case ($\mu = 1$) the kernel is more nearly

symmetric about the q–axis. In the case of low temperatures ($\mu = 10$) the kernel is shifted to positive values of q_0, since there are few high–energy particles present and the incoming photon generally loses energy to the medium.

If the incident light is a single line of frequency ω, the intensity of the scattered light is given by equation (2) as

$$S(\omega') = \mathcal{K}(\omega' \boldsymbol{u}' - \omega \boldsymbol{u}, \omega' - \omega) \tag{6}$$

For a concrete illustration, we fix the scattering angle θ to be 20^o as used in Wolf (1989). Figure 3 shows the resulting line shapes for an incoming photon with a wavelength $\lambda = 500$ nm for various values of μ. The scattering red–shifts the centroid of the line by an amount that depends on the quasi–particle mass m; the line is also broadened significantly (i.e., comparable to the shift). Figure 4a shows the width of the scattered line as a function of the wavelength of the incoming photon for different values of μ. Line widths smaller than about 100 nm can be achieved only for large values of the mass, $\mu > 50$. However, such large values suppress the intensity of the scattered light by about a factor of $e^{-\mu}$. In an astronomical context this would be an increase of some 54 magnitudes for $\mu = 50$. Figure 4b shows the red–shift of the incoming light, $z = (\lambda' - \lambda)/\lambda$ as a function of λ, the initial wavelength of the photon. The red–shift varies strongly with λ, independent of μ; this behavior is very different from the constant z characterizing a cosmological red–shift.

Finally we consider the effect of an anisotropic scattering medium. We assume an anisotropic dispersion relation for the quasiparticle of the form

$$E_k^2 = (ak_x)^2 + k_y^2 + k_z^2 + m^2 \tag{7}$$

with an asymmetry parameter a multiplying the x–component of the momentum. Such an asymmetry might arise from a magnetic field, for example. Inserting this relation into equation (4) one obtains

$$\mathcal{K}(\boldsymbol{q}, q_0) = \frac{\tilde{A}}{q\omega\omega'}\tilde{\mathcal{K}}(\tilde{\boldsymbol{q}}, q_0) \tag{8}$$

with $\tilde{\boldsymbol{q}} = (aq_x, q_y, q_z)$. Thus, the anisotropy can be accounted for by a simple rescaling of q_x and our previous formulae can be used to calculate the photon scattering from this anisotropic medium. Figure 5 shows the change of the spectrum of the scattered radiation as the anisotropy parameter a varies. Here the incident beam is again along the z–axis; i.e., orthogonal to the direction of anisotropy (x–axis). The line is shifted to larger wavelength with decreasing a. Figure 6 shows the red–shift for fixed $a = 0.4$ as a function of the photon wavelength. The scattering angle θ is fixed at 20°. The different curves shown in the plot are obtained by varying the angle θ_m between incident photon and the x–axis (in these calculations, $\boldsymbol{u}, \boldsymbol{u}'$, and the x–axis are assumed to be coplanar; i.e., $q_y = 0$). The change of the red–shift with respect to the wavelength is weaker than in the isotropic case ($a = 1$), and the width of the lines, Figure 7, is also somewhat smaller, but still quite large. Note that these results are obtained for a value of $\mu = 50$ which again leads to the strong overall suppression of the signal as discussed above.

Several conclusions can be drawn from these calculations. First, scattering from the simplest, isotropic statistical plasma cannot mimic a cosmological red–shift: the redshift is a strong function of frequency and the line is broadened by an amount comparable to the shift. These deficiencies can be ameliorated (but not eliminated) by requiring that the plasma have a high anisotropy (of order 10^3 or more) or be strongly non–relativistic ($\mu \gg 1$). However, even in such cases, the thermal distribution of plasmons strongly

suppresses the magnitude of the scattering. We also note that standard models of quasars (Rees 1989) give $n_e \lesssim 10^{10}$ cm^{-3} and $T \sim 10^4$ K, implying $\mu \lesssim 4 \times 10^{-6}$, just the opposite extreme.

Of course, our discussion cannot rule out coherent (i.e., nonstatistical) fluctuations in the plasma (as might be caused by a radio source). However, such a source would have to have a very narrow ($\sim 1\%$) bandwidth to avoid broadening the scattered line, a very unlikely circumstance. Hence, we conclude that the Wolf effect cannot be invoked to distort cosmological red–shifts.

We are grateful to Profs. G. Neugebauer and W. Sargent for drawing our attention to this problem and to Profs. S. Phinney and R. Blandford for comments on the manuscript. This work was supported in part by the National Science Foundation, Grant Nos. PHY90–13248 and PHY91–15574.

REFERENCES

Arp, H. 1987, *Quasars, Redshift and Controversies* (Berkeley, CA: Interstellar Media).

Rees, M., Netzer, H., and Ferland, G. J. 1989, *Ap. J.*, **347**, 640.

Wolf, E. 1989, *Phys. Rev. Lett.*, **63**, 2220; James, D. F. V., Savedoff, M. P., and Wolf, E. 1990, *Ap. J.*, **359**, 67; James, D. F. V. and Wolf, E. 1990, *Phys. Lett. A*, **146**, 167; see also *Sky and Telescope*, February 1992, p. 38.

FIGURE CAPTIONS

FIG. 1—Feynman graph of the photon–plasmon scattering process. The vertex Γ is assumed to have no significant momentum dependence.

FIG. 2—Contour plot of the scattering kernel $\tilde{\mathcal{K}}(q_0, q)$ when $\mu = m/T$ has the value (a) $\mu = 1$ and (b) $\mu = 10$, respectively. The dashed line in (a) shows the causal limit ($q = q_0$) beyond which $\tilde{\mathcal{K}}$ must vanish. The dash–dot line shows the energy and momentum transfer for a photon with a wavelength $\lambda = 500$ nm and a scattering angle $\theta = 20°$.

FIG. 3—Spectrum of the light scattered when the initial photon has wavelength $\lambda = 500$ nm for values of $\mu = 1, 6, \ldots, 101$. The panels (a, b, c) show the results for quasiparticle masses $m = 0.5$, 1, and 1.5 eV, respectively.

FIG. 4—(a) FWHM values and (b) red–shifts (z) of the scattered line as a function of the initial photon wavelength; values of $\mu = 6, 11, \ldots, 101$ are shown.

FIG. 5—Spectrum of the scattered light when the initial line has a wavelength of 500 nm for fixed $\mu = 50$ and values of the anisotropy parameter $a = 0.4, 0.5, \ldots, 1$.

FIG. 6—FWHM values (a) and red–shifts (b) as functions of the incident wavelength for fixed anisotropy $a = 0.004$ and $\mu = 50$. The angle between the incident photon and the anisotropy axis, θ_m, varies from 50° to 120° in steps of 10°.

Figure 1

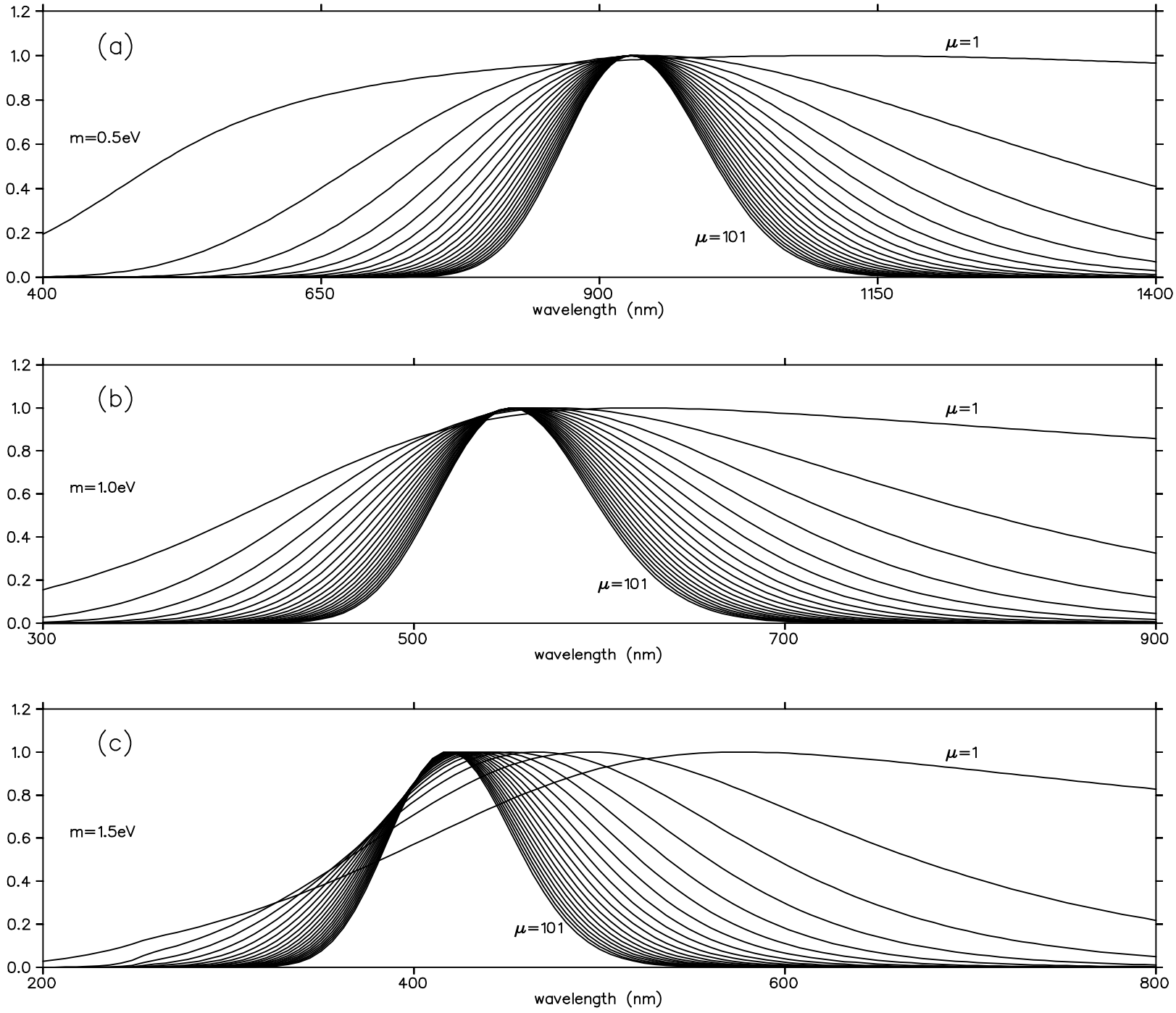
(a)
m=0.5eV
μ=1
μ=101
1.2
1.0
0.8
0.6
0.4
0.2
0.0
400
650
900
1150
1400
wavelength (nm)
(b)
m=1.0eV
μ=1
μ=101
1.2
1.0
0.8
0.6
0.4
0.2
0.0
300
500
700
900
wavelength (nm)
(c)
m=1.5eV
μ=1
μ=101
1.2
1.0
0.8
0.6
0.4
0.2
0.0
200
400
600
800
wavelength (nm)

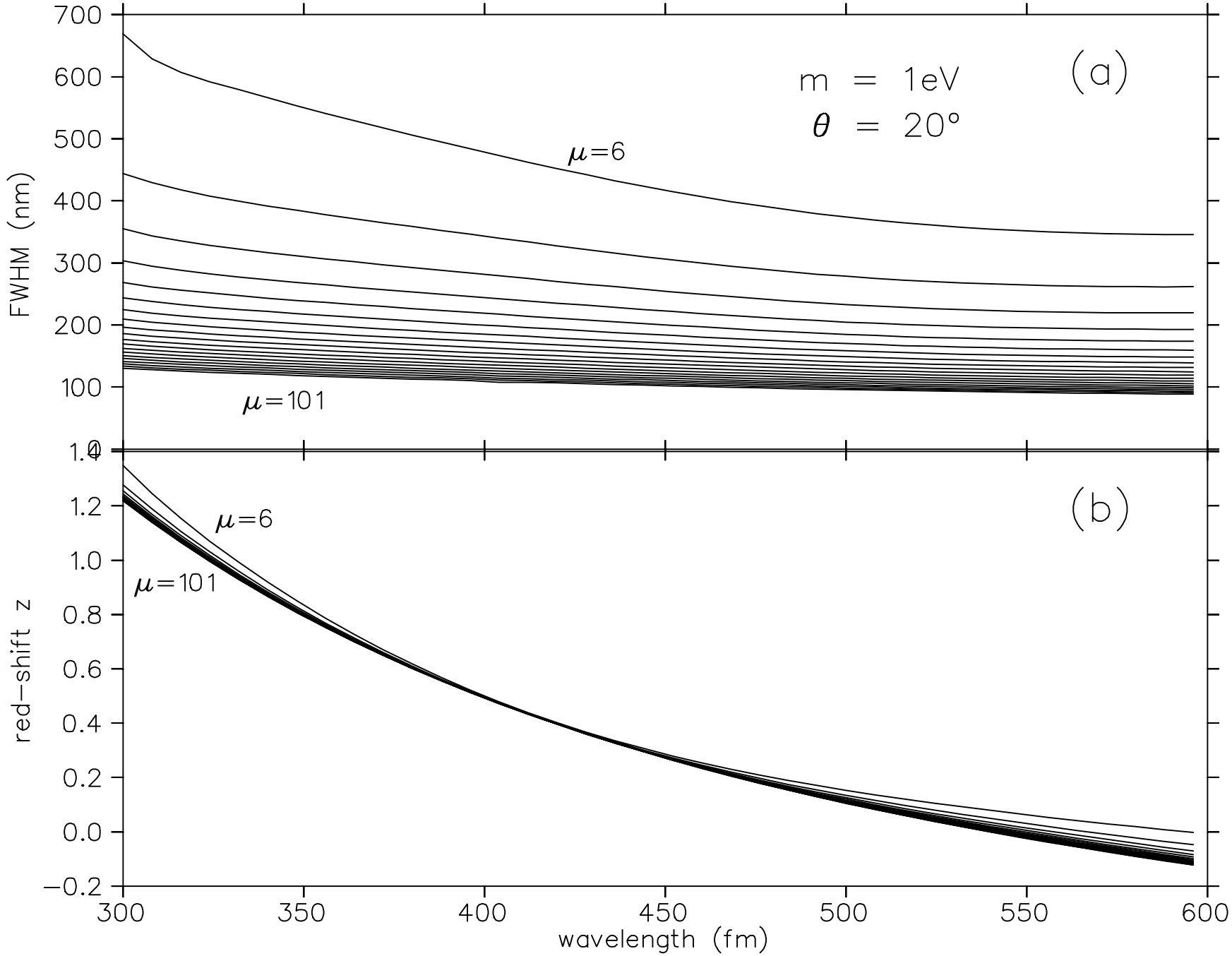
m = 1eV
θ = 20°
(a)
μ=6
μ=101
FWHM (nm)
700
600
500
400
300
200
100
(b)
μ=6
μ=101
red−shift z
1.4
1.2
1.0
0.8
0.6
0.4
0.2
0.0
−0.2
300
350
400
450
500
550
600
wavelength (fm)

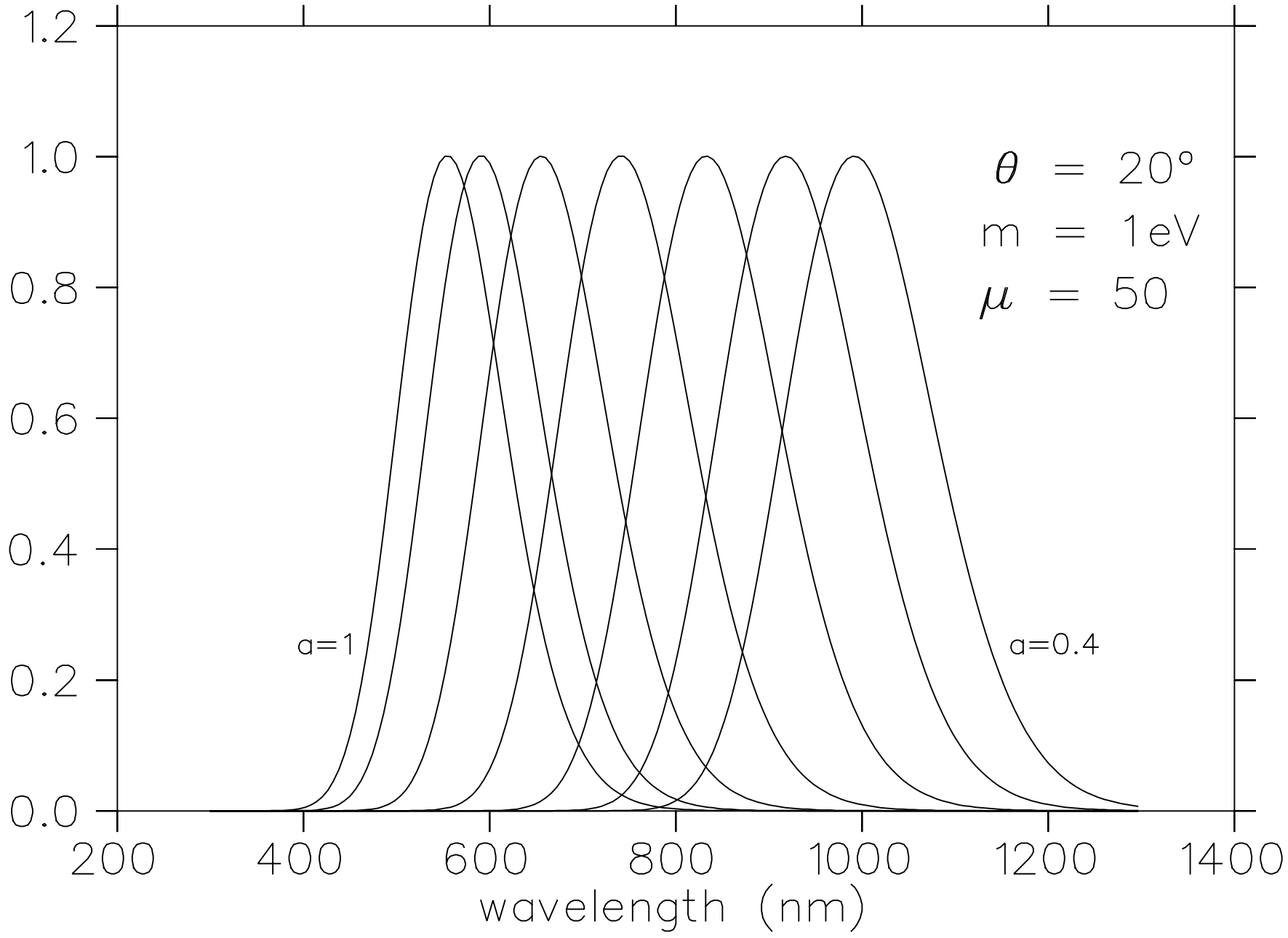
1.2
1.0
0.8
0.6
0.4
0.2
0.0
200
400
600
800
1000
1200
1400
wavelength (nm)
θ = 20°
m = 1eV
μ = 50
a=1
a=0.4

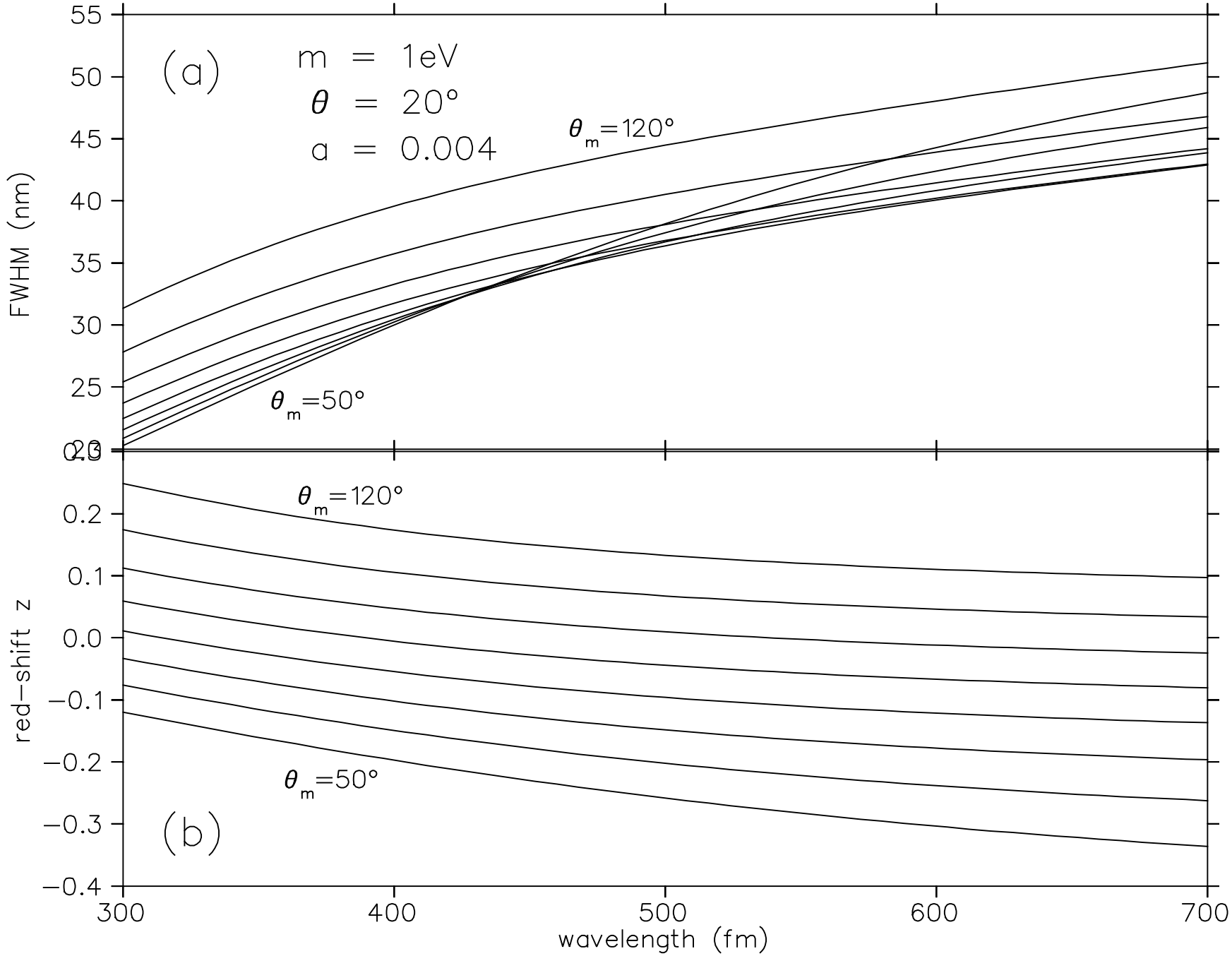
(a)
m = 1eV
θ = 20°
a = 0.004
θm=120°
θm=50°
FWHM (nm)
55
50
45
40
35
30
25
θm=120°
θm=50°
(b)
red−shift z
0.2
0.1
0.0
−0.1
−0.2
−0.3
−0.4
300
400
500
600
700
wavelength (fm)